

Research Paper

Isotopically heavy sulfur in nephelinite from Etinde, Cameroon Volcanic Line: Implications for the origin of intraplate magmatism

Sophie L. Baldwin^{a,b,*}, Linda A. Kirstein^a, J. Godfrey Fitton^a, Adrian J. Boyce^c, William Hutchison^d, Michael A.W. Marks^e, Eva E. Stüeken^d, Chris Hayward^a

^a School of GeoSciences, University of Edinburgh, James Hutton Road, Edinburgh, United Kingdom

^b British Geological Survey, Cardiff University Main Building, Park Place, Cardiff, United Kingdom

^c Scottish Universities Environmental Research Centre, Rankine Avenue, East Kilbride, United Kingdom

^d School of Earth and Environmental Sciences, University of St Andrews, Queen's Terrace, St Andrews, United Kingdom

^e Mathematisch-Naturwissenschaftliche Fakultät, Universität Tübingen, Tübingen, Germany

ARTICLE INFO

Editor: Claudia Romano

Keywords:

Sulfur isotopes

Sulfide

Sulfate

Cameroon Volcanic Line

Intraplate magmatism

Alkaline magmatism

ABSTRACT

Intraplate magmatism has traditionally been linked to anomalously hot mantle (hotspots) transported upwards from deep-sourced mantle plumes. However, many intraplate magmatic provinces lack convincing evidence for a mantle-plume origin, and the Cameroon Volcanic Line (CVL) located on the West African continental margin is one such province. Despite being active for ca. 65 million years, it lacks the time-progressive volcanic activity that would suggest the presence of a fixed mantle hotspot or plume; instead CVL magmatism has been linked to a shallow, enriched asthenospheric source. Etinde, a relatively young (<1 Ma) volcano located at the centre of the CVL on the continent-ocean boundary, is the most silica-undersaturated and incompatible element-enriched volcano in the region and forms the focus of this study. It is constructed almost entirely of feldspar-free nephelinite lava flows, with compositions ranging from olivine nephelinite to felsic leucite nephelinite. We report new sulfide-, sulfate- and bulk- $\delta^{34}\text{S}$ data for a suite of Etinde rock samples; the first sulfur-isotope data for the CVL. Strong ($\sim 8\text{‰}$) S-isotope fractionation between sulfide and sulfate (haiyne, nosean) phases suggest equilibration temperatures of $\sim 600\text{ °C}$, well below the magma solidus temperature and likely due to sub-solidus exsolution of nanoscale sulfide particles from the sulfate phenocryst phases. The most mafic samples from Etinde have been extensively degassed, containing less than 60 ppm sulfur, and therefore cannot be used to constrain the primary $\delta^{34}\text{S}$. Instead, we use the intermediate and felsic volcanic rocks, where sulfur is locked in phenocrysts of haiyne and nosean, respectively. Bulk $\delta^{34}\text{S}$ of these rocks, which best represents the primary magmatic values, ranges from $+3.7\text{‰}$ to $+6.3\text{‰}$, a heavier signature than previously reported in alkaline igneous rocks. We propose that the heavy sulfur isotope values, together with the extreme silica undersaturation and incompatible element concentrations, reflect enrichment of the mantle source and fingerprint carbonate metasomatism in the mantle beneath the CVL. The heavy sulfur isotopic signature requires low-temperature fractionation and therefore implies the addition of sulfur through subduction processes. Our study has broad geochemical significance in contributing to a growing understanding of sulfur-isotope compositional variability in geochemically enriched mantle globally.

1. Introduction

Magmatic activity that occurs away from tectonic plate boundaries has traditionally been attributed to a mantle plume source (e.g. White et al., 2025). However, controversy surrounds many intraplate magmatic provinces that lack convincing evidence of plume association, such as time-progressive volcanic activity (e.g. Geldmacher et al., 2005;

Rohde et al., 2013), excess mantle potential temperatures (e.g. Putirka, 2005; Herzberg et al., 2007) and high $^3\text{He}/^4\text{He}$ (e.g. Stuart et al., 2003). A new model proposed by Guimaraes et al. (2020) invokes the flow of carbonate- and incompatible element-enriched mantle following supercontinent break-up to explain such enigmatic intraplate magmatism. To investigate the nature of this mantle enrichment, other geochemical tracers need to be explored. Sulfur isotopes are useful in this regard as

* Corresponding author at: British Geological Survey, Cardiff University Main Building, Park Place, Cardiff, United Kingdom
E-mail address: sbald@bgs.ac.uk (S.L. Baldwin).

<https://doi.org/10.1016/j.chemgeo.2025.122748>

Received 7 January 2025; Received in revised form 14 March 2025; Accepted 17 March 2025

Available online 18 March 2025

0009-2541/© 2025 The Authors. Published by Elsevier B.V. This is an open access article under the CC BY license (<http://creativecommons.org/licenses/by/4.0/>).

they are strongly fractionated in near-surface (low-temperature) environments and are not fractionated significantly during magma evolution by fractional crystallisation of silicate phases. Here we show that Etinde (Fig. 1), one of the volcanoes comprising the Cameroon Volcanic Line (CVL) provides a unique opportunity to apply sulfur-isotope geochemistry to the problem of the origin of enigmatic intraplate magmatism.

Sulfur isotopes can be used to track mantle sulfur cycling and can potentially provide useful information about mantle-enrichment processes, but $\delta^{34}\text{S}$ can be modified by isotopic fractionation during shallow magmatic processes, such as degassing, assimilation or mixing, and sulfide segregation (De Moor et al., 2013; Beaudry et al., 2018; Dottin et al., 2020; Saal and Hauri, 2021). The extent of these must be evaluated in order to determine which $\delta^{34}\text{S}$ values best reflect the $\delta^{34}\text{S}$ of the original melt. After accounting for these processes, sulfur isotope measurements have been used to invoke mantle enrichment via ancient crustal recycling at Samoa (Labidi et al., 2015; Dottin et al., 2020), Discovery Seamounts (Labidi et al., 2013) and Mangaia (Cabral et al., 2013) and mantle metasomatism at the Gardar Province in Greenland (Hutchison et al., 2019, 2021).

We have measured the sulfur isotope ratios of both the sulfate and sulfide components in a suite of Etinde samples to estimate the whole-rock $\delta^{34}\text{S}$. We compare our data with the well-constrained normal asthenospheric mantle $\delta^{34}\text{S}$ value of -2.0‰ to -1.0‰ (Labidi et al., 2012); this range is determined from measurements of MORB glasses, which suggest that normal asthenospheric $\delta^{34}\text{S}$ is fairly constant. We discuss the potential $\delta^{34}\text{S}$ signature associated with carbonate metasomatism at the CVL and evaluate the effect of assimilating evaporite (e.g. anhydrite) on bulk $\delta^{34}\text{S}$. We also discuss inter-sample $\delta^{34}\text{S}$ variability and address potential magmatic processes, such as degassing, that might affect this.

2. Geological setting

The Cameroon Volcanic Line (CVL) is a 1600 km-long intraplate magmatic province that spans the passive continental margin of West Africa (Fitton, 1987). Despite being magmatically active for ca. 65 million years, the CVL lacks linear age-progression, and the youngest magmatic activity (the recently active Mt. Cameroon) is located in the centre of the line (Fitton and Dunlop, 1985; Njome and De, 2014). The absence of fault-bounded graben show that the CVL was not formed by lithospheric extension. There are no primordial geochemical mantle signatures, such as high $^3\text{He}/^4\text{He}$ or $^{20}\text{Ne}/^{22}\text{Ne}$, recorded at the CVL (Barfod et al., 1999, Class and Goldstein, 2005), the presence of which is often associated with a mantle plume origin. Furthermore, the CVL was identified as one of four ‘cold hotspots’ in a recent compilation of global temperature estimates based on seismic velocity (Bao et al., 2022).

Etinde, which forms the focus of this study, is a young ($< 1\text{ Ma}$) volcano of the CVL. It is located at the ocean-continent boundary zone, close to the centre of the CVL, and is partly enveloped by more recent alkali basalt and basanite lava flows from the much larger Mount Cameroon (Fig. 1). The rock samples used in this study were collected from boulders in streams and rivers running down the southwest flank of Etinde. Rivers and streams on the sides of Etinde are isolated from other drainage networks such as those on Mount Cameroon because Etinde forms a topographic high, meaning these boulders can only have come from Etinde. Dense rainforest precludes in situ sampling of the lava flows, although Nkoumbou et al. (1995) have published a geological sketch map based on the very limited exposure available. The Etinde rock suite consists almost entirely of feldspar-free nephelinites ranging in composition from mafic (olivine-phyric) to felsic (schorlomite- $(\text{Ca}_3\text{Ti}_2(\text{SiO}_4)(\text{Fe}^{3+}\text{O}_4))$ and nosean-phyric), and is highly enriched in incompatible elements (Fitton, 1987; Nkoumbou et al., 1995; Ntombé

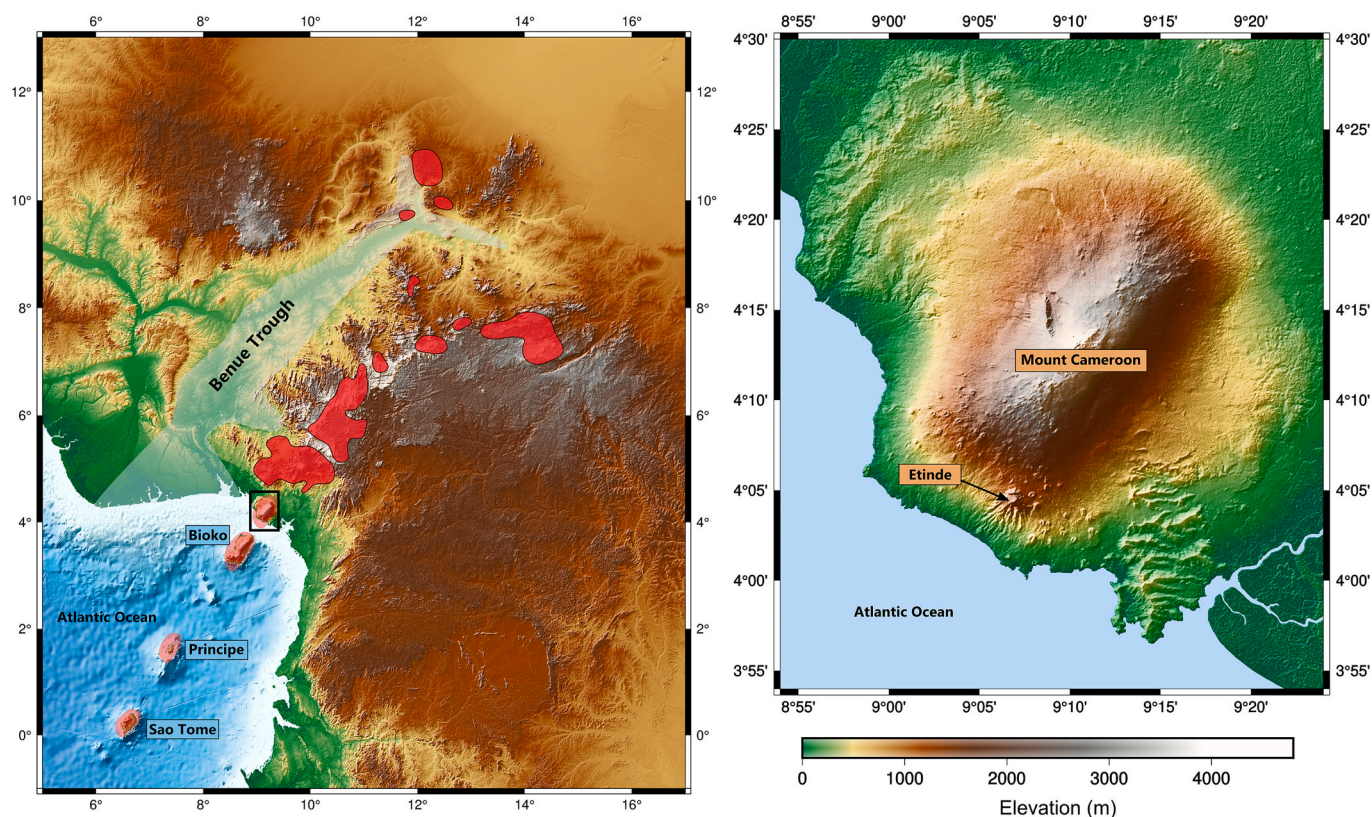


Fig. 1. Topographic maps showing the location of the Cameroon Volcanic Line (CVL) and Etinde. The dark red areas on the left map show the locations of the continental volcanic rocks of the CVL. The four islands (coloured pink) form the oceanic sector of the CVL. The black rectangle shows the location of the enlarged map to the right which highlights the location of Etinde partly enveloped by younger lavas from Mount Cameroon. Maps produced using PyGMT after Wessel et al. (2019) and Tian et al. (2023). (For interpretation of the references to colour in this figure legend, the reader is referred to the web version of this article.)

et al., 2016). The compositionally intermediate and felsic nephelinites usually contain abundant phenocrysts of haiyine ($\text{Na}_3\text{Ca}(\text{Si}_3\text{Al}_3)\text{O}_{12}(\text{SO}_4)$) or nosean ($\text{Na}_8\text{Al}_6\text{Si}_6\text{O}_{24}(\text{SO}_4)\cdot\text{H}_2\text{O}$), respectively. These silicate phases host volatiles, such as sulfur and chlorine, in their structure and so are particularly informative when characterising volatile enrichment in silica-undersaturated magmas (Baudouin and Parat,

2015).

The Etinde rock samples represent a co-magmatic suite related by fractional crystallisation (Nkoumbou et al., 1995). The various members of the Etinde suite are indistinguishable in their Sr, Nd and Pb isotope ratios from each other and from the neighbouring Mount Cameroon basanite and alkali basalt lavas (Halliday et al., 1990). Reported

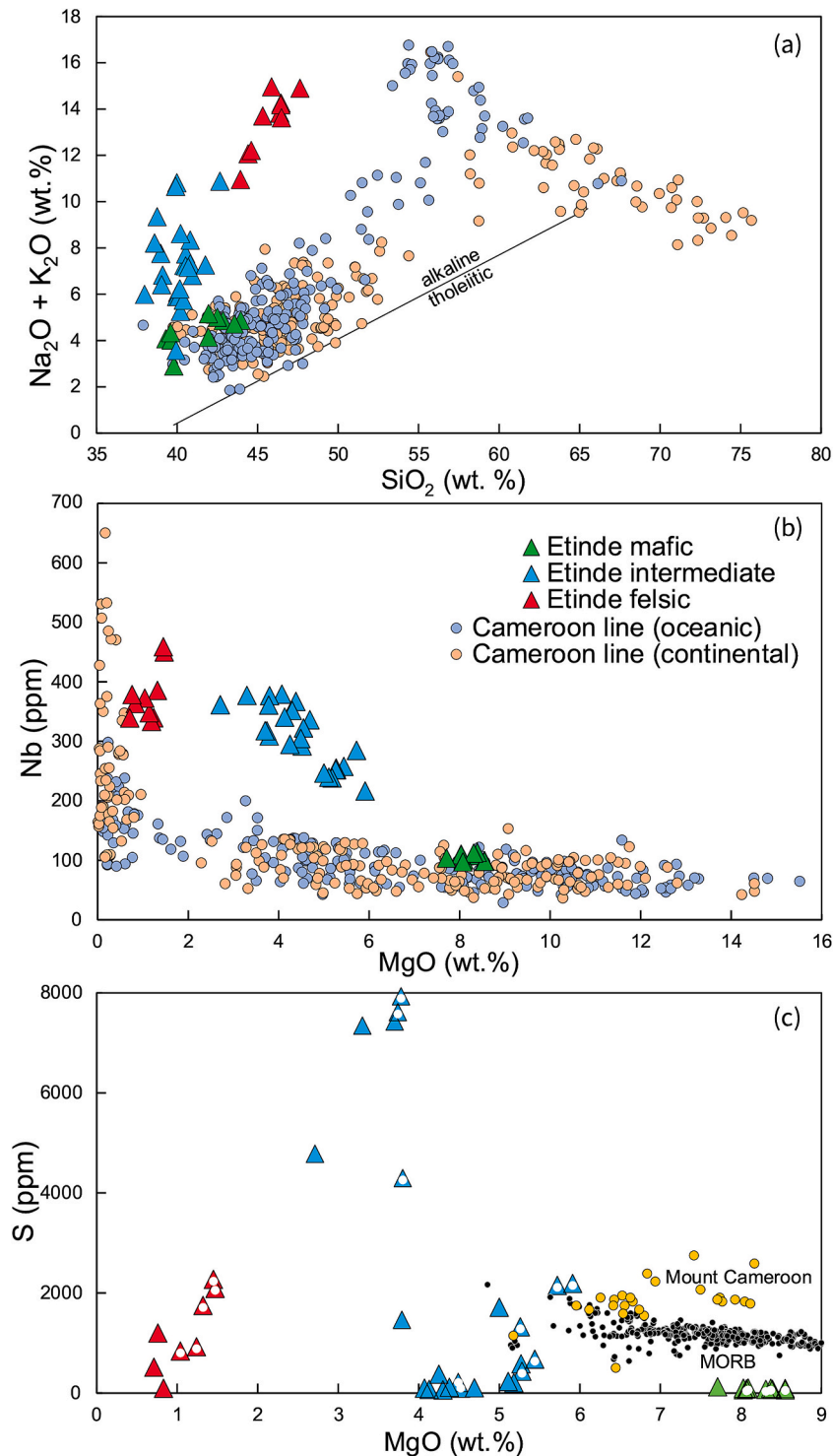


Fig. 2. (a) A total alkali–silica diagram showing the highly silica-undersaturated character of the Etinde lava flows compared with volcanic rocks from the rest of the CVL. The line separating alkaline and tholeiitic compositions is from Macdonald and Katsura (1964). (b) and (c) The variation of Nb and S, respectively, with MgO content in the Etinde samples. Data from the rest of the CVL are shown on (b) for comparison. Etinde data points are colour-coded by group (mafic, intermediate, felsic). The white circles within the data points in (c) identify those samples used in the present study (Table 1). MORB data in (c) are from Jenner and O'Neill (2012) and the Mt. Cameroon data are from Suh et al. (2008). Analytical uncertainty (2σ) is within the size of the data points on all diagrams.

radiogenic-isotope data at Etinde and other volcanos of the CVL show no indication of crustal contamination (Halliday et al., 1990). The strong enrichment in volatile and incompatible elements in the Etinde magmas cannot be explained solely by small-degree melting of normal asthenospheric mantle. For example, niobium concentrations vary from ~100 ppm in the most mafic (primitive) samples (MgO ~ 8 wt%) to >400 ppm in the more felsic (evolved) samples (MgO ~ 2 wt%; Fig. 2), compared to <10 ppm in mid-ocean ridge basalt (MORB) and ~ 50 ppm in typical ocean island basalt (OIB) (Sun and McDonough, 1989). If the most primitive Etinde magmas had undergone 20 % crystallisation of olivine before eruption, their primary melt would have contained about 80 ppm Nb. To produce a primary melt of this composition from primitive mantle with 0.64 ppm Nb (Macdonald and Katsura, 1964) would require a melt fraction of ~0.8 %. Some prior enrichment of the mantle source, as proposed by Guimarães et al. (2020), is required. These authors argue that the Cameroon line was fed over long time periods with enriched asthenospheric mantle flowing out from beneath Africa following the breakup of Gondwana. The enriched asthenosphere is suggested to be formed by the thermal re-equilibration and mobilisation of enriched lithospheric mantle, which was thickened during supercontinent assembly. The base of the lithospheric mantle is likely enriched in volatile and incompatible elements by the upward percolation and freezing of carbonate-rich, small-degree melts generated at the intersection of the geotherm with the CO₂-saturated mantle solidus (McKenzie, 1989).

3. Methods

3.1. Whole-rock geochemistry

Whole-rock powders were made by grinding rock samples in a Tema mill with a tungsten carbide barrel. Major- and trace-element compositions were determined by X-ray fluorescence (XRF) spectrometry on whole-rock powders at the University of Edinburgh. XRF methods and analytical precision data are given in Fitton et al. (1998). XRF analyses of the Etinde rock suite are given in a Supplementary Data file.

Sulfur concentrations were measured using combustion ion-chromatography (CIC) at Universität Tübingen (Eggenkamp et al., 2020). Full details for the techniques are provided in the Supplementary Material.

3.2. Isotope analysis

To measure $\delta^{34}\text{S}$ in the sulfate phases, sulfur was extracted via an acid-based dissolution and precipitation method after Renzulli et al. (1998). This sample preparation was undertaken at the School of Geo-Sciences, University of Edinburgh. Approximately ~20 g of whole-rock powder was leached with 50 ml of 2.5 M hydrochloric acid (HCl), stirred, and placed on a hotplate at 50 °C overnight. The suspension was then filtered and three drops of 12 M HCl were added to the filtered solution. Five drops of a 5 % barium chloride (BaCl₂) solution were stirred in, leading to precipitation of barium sulfate (BaSO₄). This was then decanted and rinsed in distilled water, before being separated by filtration. Nanoscale monosulfide inclusions in sulfate phases react with HCl in this type of digestion; however this produces H₂S, which is not precipitated as barium sulfate. Pyrite sulfide is insoluble in 2.5 M HCl (Canfield et al., 1986). The $\delta^{34}\text{S}$ of the sulfate component was measured at the Scottish Universities Environmental Research Centre, East Kilbride following the method of Coleman and Moore (1978). Liberated SO₂ gases were analyzed on a VG Isotech SIRA II mass spectrometer, and standard corrections applied to raw $\delta^{66}\text{S}_{\text{O}_2}$ values to produce true $\delta^{34}\text{S}$ values. Data are reported in $\delta^{34}\text{S}$ notation as per mil (‰) variations from the Vienna Cañon Diablo Troilite (V-CDT) standard. The calibration standards used were the international standards NBS-123 (ZnS, accepted value 17.4 ‰) and IAEA-S-3 (Ag₂S, -32.5 ‰), and SUERC standards CP-1 (CuFeS₂, -4.6 ‰) and NBS-127 (BaSO₄, 21.1 ‰). Repeat analyses of these standards gave $\delta^{34}\text{S}$ values of $+17.3 \pm 0.2$ ‰, -32.3 ± 0.2 ‰,

-4.6 ± 0.2 ‰ and $+21.3 \pm 0.2$ ‰, respectively, around the time our samples were processed.

Sulfide was extracted from whole-rock powders using a Cr reduction procedure at the University of St Andrews following Canfield et al. (1986). Approximately 20 g of whole-rock powder was used for each sample, with the exact quantity recorded to facilitate yield calculations after extraction. A 50 % solution of HCl was added to the powder in a system flushed with N₂ to release acid-volatile sulphide (AVS) which can form following chemical weathering or as a secondary sulphide after pyrite formation (not applicable in these rocks). Following the addition of HCl, the AVS reacts to form H₂S gas, which is condensed and combined with silver nitrate solution to precipitate silver sulphide which was collected for analysis. In order to determine chromium-reducible sulfide (CRS) in the sample, an acidified 1 M chromium chloride (CrCl₂) solution was added to the residual rock powder and the mixture boiled. H₂S gas was released and once more combined with silver nitrate solution to produce a second silver sulfide precipitate for analysis. The $\delta^{34}\text{S}$ value for both of the sulfide components was measured at the Department of Chemistry at the University of St Andrews. An EA IsoLink, coupled to a MAT 253 IRMS was used. Standard deviation of sample replicates was 0.2 ‰. The calibration standard used was NBS-127 and four repeat analyses of this standard gave $\delta^{34}\text{S}$ values of $+21.57 \pm 0.18$ ‰ which agrees well with the expected value.

Bulk sulfide $\delta^{34}\text{S}$ was calculated by mass-balance from measured acid-volatile and chromium-reducible sulfide components. Mass balance was also used to calculate bulk $\delta^{34}\text{S}$ from sulfide and sulfate $\delta^{34}\text{S}$. Elemental sulfur and sulfur-isotope data are given in Table 1.

3.3. Sulfur speciation

The speciation of sulfur in h aüyne and nosean phenocrysts was investigated by electron microprobe analysis following Hettmann et al. (2012) with the CAMECA SX100 at the University of Edinburgh. The SK a peak was carefully scanned using a PET analysing crystal, and sphalerite, pyrite and celestite standards allowed our calculated eV values for SK a to be calibrated against the values given by Hettmann et al. (2012). Further details on the methods, techniques and equipment are available in Supplementary Material.

4. Results

4.1. Major and trace element data

The Etinde nephelinites are strikingly more silica-undersaturated from the rest of the CVL volcanic rocks, as can be seen on a total alkali-silica diagram (Fig. 2a). Three rock sub-groups are defined petrographically for the Etinde samples: the olivine-phyric mafic group; a suite of intermediate nephelinites, most of which contain h aüyne phenocrysts; and the felsic group comprising schorlomite- and nosean-phyric nephelinites.

The mafic group have the highest MgO content (>8 wt%), and lowest total S (< 60 ppm), Nb (~100 ppm) and Zr (~350–410 ppm) compared to the other groups (Fig. 2b, c). The mafic samples represent the most primitive magmas as they have the highest MgO and the lowest Nb and Zr contents. A key observation is that these samples all contain <60 ppm total sulfur, much lower than expected in mafic alkaline magmas (~2400 ppm; Hutchison et al., 2019). The intermediate samples have MgO contents of 2.7–5.9 wt%, total S ~ 150–8000 ppm, Nb ~200–380 ppm and Zr ~600–1000 ppm. The notable variation in total sulfur (Fig. 2c) is related to the variable abundance of S-rich h aüyne phenocrysts. Finally, the felsic samples have MgO <1.5 wt%, total S from 250 to 2400 ppm, Nb of ~310–450 ppm and Zr content between 880 and 1000 ppm. The lowest MgO content and highest Nb and Zr contents show that the felsic group comprises the most geochemically evolved samples, consistent with the samples being related by fractional crystallisation.

Table 1

Sulfur isotope data and MgO, S, Nb and Zr contents of samples measured in this study. Samples are presented in order of decreasing MgO content. Where a % sulfide appears with no $\delta^{34}\text{S}$ sulfide data, the precipitate yielded during sulfide extraction could not be measured.

Sample type and ID	$\delta^{34}\text{S}$ sulfate (‰)	$\delta^{34}\text{S}$ AVS (‰)	$\delta^{34}\text{S}$ CRS (‰)	$\delta^{34}\text{S}$ sulfide (‰)	sulfide yield (%)	$\delta^{34}\text{S}$ bulk (‰)	MgO (wt%)	S (ppm)	Nb (ppm)
Mafic, C219	–	–	–	–	6.1	–	8.55	51	100
Mafic, C225	–	–	–0.60	–0.60	27.3	–0.60	8.37	55	108
Mafic, C221	–	–	–0.05	–0.05	10.4	–0.05	8.31	32	112
Mafic, C214	–	–3.4	–	–3.4	8.5	–3.4	8.09	59	101
Mafic, C222	–	–	–	–	1.8	–	8.07	43	97
Int, C228	+5.8	–5.2	–	–5.2	1.9	+5.6	5.91	2151	216
Int, C127	+4.1	–	–	–	–	–	5.72	2111	285
Int, C229	+4.8	–5.8	–3.0	–5.3	0.9	+4.7	5.44	636	258
Int, C24	+4.4	–4.5	–2.3	–4.3	7.7	+3.7	5.28	394	252
Int, C22	+4.4	–	–	–	–	–	5.26	1282	253
Int, C33	–	–	–	–	0	–	4.52	97	292
Int, C227	–	–	–	–	0	–	4.49	208	305
Int, C215	+4.8	–	–	–	–	–	3.80	4258	377
Int, C126	+3.9	–	–	–	–	–	3.78	7890	361
Int, C152	+4.2	–	–	–	–	–	3.74	7575	318
Felsic, C217	+6.9	–	–	–	–	–	1.47	2052	450
Felsic, C216	+6.1	–	–	–	–	–	1.45	2233	459
Felsic, C231	+6.7	–3.8	–0.91	–1.1	24.5	+4.8	1.32	1710	386
Felsic, C230	+5.1	–	–	–	–	–	1.24	884	340
Felsic, C218	+8.1	–0.8	–1.2	–1.2	19.2	+6.3	1.04	799	373

4.2. Sulfur isotope data

Sulfate $\delta^{34}\text{S}$ measured in thirteen intermediate and felsic Etinde nephelinite samples ranges from +3.9 ‰ to +8.1 ‰ (Fig. 3) and increases slightly with decreasing MgO content (Fig. 4). Bulk sulfide $\delta^{34}\text{S}$ compositions were obtained for ten Etinde samples ranging from mafic to felsic in composition. Bulk sulfide $\delta^{34}\text{S}$ is made up of mass-balanced acid-volatile (AVS) and chromium-reducible sulfide (CRS) components, where the former primarily comprises monosulfides, and the latter disulfides. The exact sulfide phases present could not be determined in any of the samples as the sulfide grains were too small to be viewed with optical microscopy or analyzed using microbeam techniques. Two intermediate samples (C33 and C227) yielded too little sulfur for isotope analysis (Table 1). Sulfide $\delta^{34}\text{S}$ is lower than sulfate $\delta^{34}\text{S}$ in all samples where both phases are present, and ranges from –5.3 ‰ to –0.05 ‰. There is no clear relationship between sulfide $\delta^{34}\text{S}$ and MgO content (Fig. 4). Bulk rock $\delta^{34}\text{S}$ does not correlate with sulfur content (Fig. 4, Table 1).

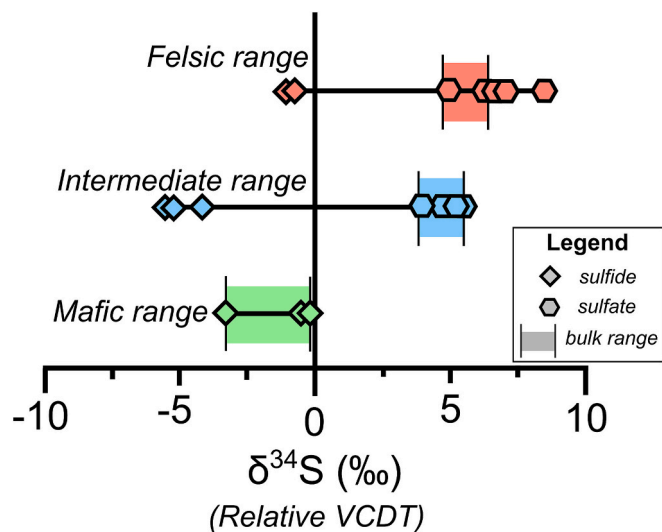


Fig. 3. $\delta^{34}\text{S}$ for the mafic, intermediate and felsic Etinde samples. The range in calculated bulk rock $\delta^{34}\text{S}$ is shown in the shaded zones, the $\delta^{34}\text{S}$ values of the sulfide and sulfate components of samples from each group are also shown with diamonds and hexagons, respectively. Error in isotope compositions is 0.2 ‰.

The bulk-rock $\delta^{34}\text{S}$ values in the felsic and intermediate samples were calculated by mass-balance. Specifically, a percentage yield of the sulfur hosted as sulfide was calculated after the sulfide component was extracted from whole rock powder and weighed. This facilitated calculation of bulk rock $\delta^{34}\text{S}$ by combining $\delta^{34}\text{S}_{\text{sulfide}}$ and $\delta^{34}\text{S}_{\text{sulfate}}$ such that: $\% \text{ sulfide} = \text{measured } \% \text{ yield sulfide}$ and: $\% \text{ sulfate} = 100 - \% \text{ yield sulfide}$. To do this, we assumed that the sulfide extraction technique is fully efficient and that, as these rocks are fully crystalline, there is no unextractable sulfate hosted in glass. For the felsic and intermediate samples, there are sulfate-bearing phenocrysts present, and the sulfide yield is <25 %, meaning the bulk $\delta^{34}\text{S}$ values are dominated by the sulfate component (Fig. 3). The bulk $\delta^{34}\text{S}$ of the mafic samples is taken to be the sulfide $\delta^{34}\text{S}$ value because, unlike the intermediate and felsic samples, there is no sulfate-bearing mineral phase present in any sample of this group.

Bulk rock $\delta^{34}\text{S}$ ranges from –3.4 ‰ to +6.3 ‰ and increases with decreasing MgO content (Fig. 4). All of the mafic samples have bulk $\delta^{34}\text{S}$ compositions below 0 ‰. In the discussion, we evaluate which samples are most representative of the melts from which they formed, and hence of most use for understanding the melt source region, and which samples may have been influenced by subsequent magmatic processes.

5. Discussion

5.1. $\delta^{34}\text{S}$ in the Etinde mafic magma

The mafic Etinde samples in this study have conspicuously low sulfur contents, ranging from 32 to 59 ppm. By comparison, the S content of MORB glasses rises from ~800 to ~2000 ppm with falling MgO content (Jenner and O'Neill, 2012; Fig. 2c). A recent study of volatile-elements in olivine-hosted melt inclusions in OIB (Kirstein et al., 2023) reported values of up to 2619 ppm S, while inclusions from El Hierro, Canary Islands, contain up to 4290 ppm (Taracsák et al., 2019). Olivine-hosted melt inclusions from Mount Cameroon (Fig. 1) have S contents that range up to 2700 ppm (Suh et al., 2008; Fig. 2c), and melt inclusions from the Central African alkaline volcano Nyamuragira have similar concentrations (Head et al., 2012). It is therefore reasonable to assume that the primitive Etinde magma initially contained around 2400 ppm S, and that the mafic samples have lost ~98 % of their sulfur through degassing before or during eruption.

Large amounts (>50 %) of degassing can significantly fractionate sulfur isotopes, though the effect on $\delta^{34}\text{S}$ is strongly dependent on $f\text{O}_2$ (Fig. 5) (Beaudry et al., 2018 and references therein). This may explain

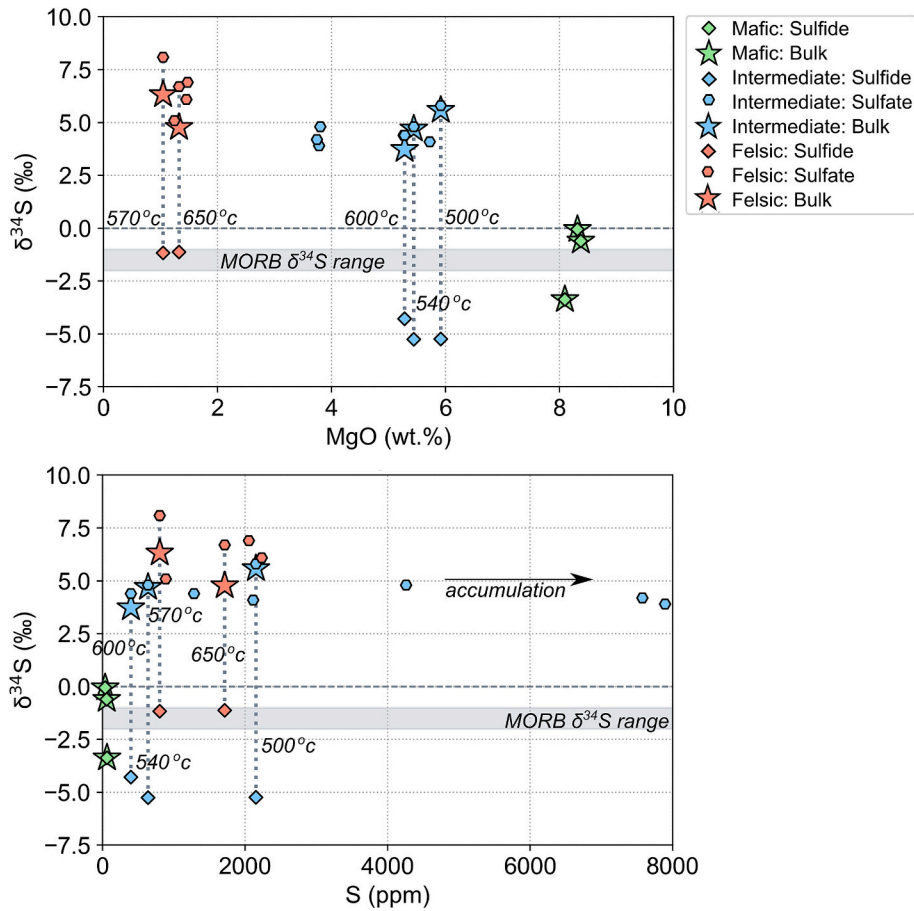


Fig. 4. Sulfide (diamonds), sulfate (hexagons) and bulk (stars) $\delta^{34}\text{S}$ values plotted against whole-rock a) MgO and b) sulfur content. Grey shaded rectangles show the $\delta^{34}\text{S}$ range for MORB using values from Labidi et al. (2012). The arrow on the lower plot shows the effect on S content of accumulation of haüyne and nosean phenocrysts by flotation in the magma. The numbers beside the intermediate and felsic samples show calculated isotopic equilibrium temperatures based on the difference in $\delta^{34}\text{S}$ between sulfate and sulfide. These temperatures are calculated based on a model for $\text{SO}_4\text{-H}_2\text{S}$ fractionation presented in Eldridge et al. (2016) (see Section 4.3). Error in isotope compositions is 0.2 ‰. Error in whole-rock MgO and S content is within the size of the symbol used.

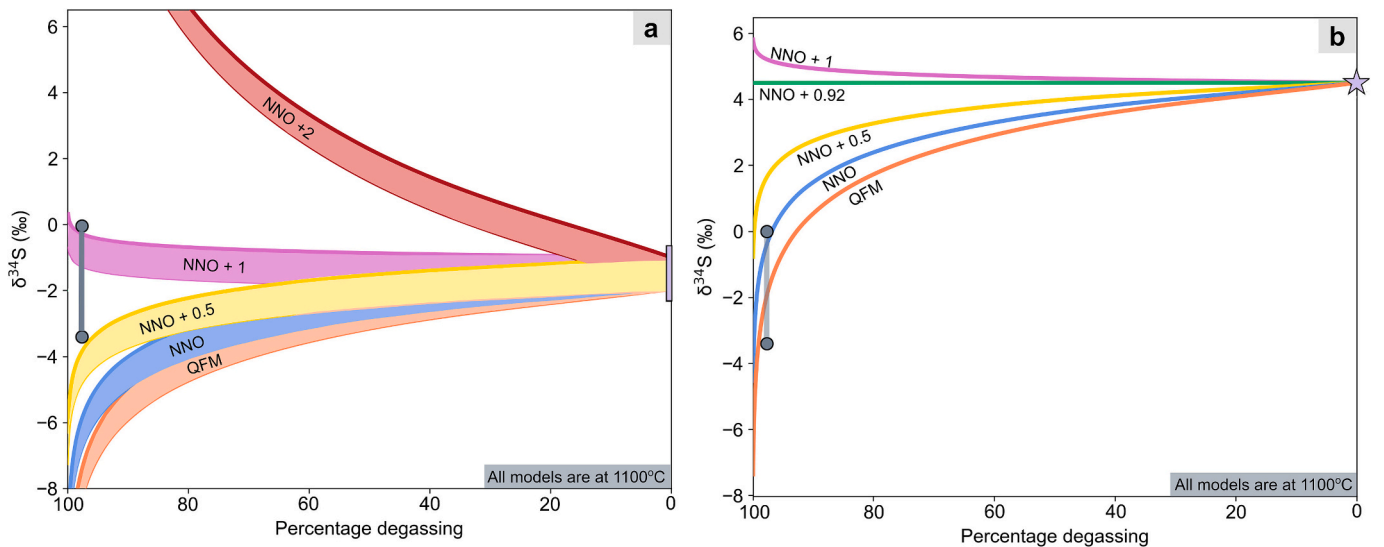


Fig. 5. The effect on $\delta^{34}\text{S}$ of magma degassing at 1100 °C with varied f_{O_2} and initial S content of 2400 ppm with: a) MORB-like $\delta^{34}\text{S}$ of -2.0 ‰ to -1.0 ‰, b) $\delta^{34}\text{S}$ comparable with that in the intermediate and felsic rocks ($+4.5$ ‰). The range in $\delta^{34}\text{S}$ of the mafic samples is shown by the grey vertical bar. The <60 ppm S content of the mafic samples implies that they are at least 98 % degassed. Calculations are based on the technique of Marini et al. (1998) and are provided as an open access Jupiter notebook (see Data Availability).

the difference in $\delta^{34}\text{S}$ between the mafic ($\sim -2\%$) and intermediate/felsic ($\sim +5\%$) samples, assuming that the intermediate magmas were derived by fractional crystallisation from the mafic nephelinite magma and that $\delta^{34}\text{S}$ was unaffected by this process. Fractionation of sulfides could, in principle, reduce S content and $\delta^{34}\text{S}$ values (e.g. Labidi et al., 2015) but if the intermediate and felsic magmas have evolved via fractional crystallisation from the mafic magma, the high S content of the former would be hard to explain if sulfur had been lost by separation of sulfides from the latter.

In an attempt to explain the low S and $\delta^{34}\text{S}$ in the mafic nephelinites, we modelled open-system degassing of the Etinde magmas by applying the procedures described by Marini et al. (1998). All models were run at a temperature of 1100 °C, though models run up to 1200 °C showed very similar results. First, we consider the possibility that degassing of mafic magma with initial MORB-like $\delta^{34}\text{S}$ (-2.0% to -1.0%) and S content of 2400 ppm could leave $\delta^{34}\text{S}$ unaffected and that the measured values in the mafic rocks represents that in the undegassed magma. The results of the model (Fig. 5a) show that degassing under the most likely range of $f\text{O}_2$ (between the FMQ and NNO buffers; see e.g. Moussallam et al., 2019) would reduce $\delta^{34}\text{S}$. For the mafic magmas to retain their measured value would require $f\text{O}_2$ between NNO + 0.5 and + 1; values considerably higher than the average value in OIB (FMQ + 0.5; Willhite et al., 2024), although these authors note that their estimated $f\text{O}_2$ in some OIB do extend to these high values.

The results of modelling an undegassed magma with $\delta^{34}\text{S}$ of +4.5‰ and S content of 2400 ppm is shown in Fig. 5b. The low sulfur content and $\delta^{34}\text{S}$ composition of the mafic samples could have resulted from $\sim 98\%$ degassing at $f\text{O}_2$ around FMQ to NNO of a magma with the high $\delta^{34}\text{S}$ of the intermediate and felsic samples. O'Neill and Mavrogenes (2022) have shown that degassing of SO_2 is strongly $f\text{O}_2$ -dependent and most efficient in magmas with $\text{Fe}^{3+}/\text{Fe}^{2+} = 0.2$. The least oxidised lava samples from the adjacent Mt. Cameroon have $\text{Fe}^{3+}/\text{Fe}^{2+} = 0.32$ (Suh et al., 2008), but this is likely a maximum value for the magma. Applying eq. 8.2 of Berry and O'Neill (2022) to a magma with $\text{Fe}^{3+}/\text{Fe}^{2+} = 0.2$ and the CaO, MgO, Na₂O and P₂O₅ contents of our mafic nephelinites gives $f\text{O}_2$ equivalent to FMQ + 1.06 (NNO + 0.26). This is slightly higher than that required by our model to replicate the low $\delta^{34}\text{S}$ in our mafic samples; to have $f\text{O}_2 < \text{NNO}$ would require $\text{Fe}^{3+}/\text{Fe}^{2+} < 0.216$ ($\text{Fe}^{3+}/(\text{Fe}^{2+} + \text{Fe}^{3+}) < 0.18$). This is not an unreasonably low value for mafic alkaline magmas and is still close to the value required for optimum degassing of SO_2 (O'Neill and Mavrogenes, 2022).

We conclude that the mafic Etinde lava samples have lost sulfur by $>95\%$ degassing and that, as a consequence, their $\delta^{34}\text{S}$ values can't be taken as that of the primitive Etinde magmas. This is best represented by the intermediate and felsic samples ($\delta^{34}\text{S} \sim +5.0\%$). The mafic, intermediate and felsic rocks form a co-magmatic suite related by fractional crystallisation of silicate phases; a process that would not fractionate sulfur isotopes significantly (Marini et al., 2011).

5.2. $\delta^{34}\text{S}$ in the Etinde intermediate and felsic magmas

The $\delta^{34}\text{S}$ values of the intermediate and felsic samples (MgO < 6 wt %) reliably reflect the undegassed magmatic $\delta^{34}\text{S}$ of the melt from which they crystallised because almost all of the sulfur in these samples is hosted in h a yne and nosean phenocrysts, phases that contain structurally bound sulfur. The elevated sulfur contents in intermediate samples C215, C126 and C152 (Table 1; Fig. 4b) is due to accumulation of h a yne phenocrysts, a process evident from sample petrography. The large size and euhedral morphology of these crystals, and their occasional presence as inclusions in titanite phenocrysts, indicate that they clearly crystallised on or near the magma liquidus temperature. Studies on the Lacher See tephros (Eifel, Germany) and h a ynophyre lavas of Vulture (Italy) show that h a yne crystallised between 1150 and 1255 °C in these magmatic systems (Baudouin and Parat, 2015). These rocks are broadly comparable to the Etinde lavas in their compositions and mineral assemblages. At these magmatic temperatures, isotopic

fractionation has little effect as fractionation factors vary inversely with the square of temperature (e.g. Marini et al., 2011). As such, the phenocrysts record and retain the $\delta^{34}\text{S}$ of the melt at the time of crystallisation and are unaffected by subsequent magmatic processes, such as degassing on eruption that can fractionate S-isotopes.

Petrographic examination of the rock samples in reflected light failed to reveal any visible sulfide phases. In some felsic samples, however, the sulfide yield on acid extraction was up to $\sim 25\%$ of the total sulfur. An explanation for this lies in the dark brown rims and cores of the sulfur-rich h a yne and nosean crystals, respectively (Fig. 6) which are most likely caused by the exsolution of sub-microscopic particles of a sulfide phase. This was confirmed by electron microprobe wavelength-dispersive scans using a PE analysing crystal in order to measure SK  peak shifts, which reflect the oxidation state of the sulfur (Hettmann et al., 2012). These scans are given in the Supplementary Material. The scans for a h a yne phenocryst in C228 (Fig. 6) show an increase of 0.233 eV from core to rim, implying that the rim has a higher proportion of sulfur as sulfide than does the core. For a nosean phenocryst in C231 (Fig. 6), the SK  peak is shifted 0.117 eV lower from core to rim, suggesting that the cores have a higher proportion of sulfide than do the rims. These differences, though small, are accurate, given the excellent angular precision of electron microprobe goniometers.

In the intermediate and felsic samples, all of the sulfides are present as sub-microscopic particles in h a yne and nosean phenocrysts, as the only two samples (C33 and C127) from these groups that are free of these phases also yielded no detectable sulfide or sulfate (Table 1). It is likely that the h a yne and nosean phenocrysts contained sulfide bound in the silicate lattice at the temperature of crystallisation and that the sulfide particles exsolved on cooling. The difference in $\delta^{34}\text{S}$ between sulfide and sulfate phases is likely a function of the temperature of final equilibration. The magnitude of the difference between the $\delta^{34}\text{S}$ of the sulfide and sulfate components can therefore be used to calculate equilibrium temperatures based on $\text{SO}_4^{2-} - \text{H}_2\text{S}$ fractionation (Eldridge et al., 2016). Calculated equilibrium sulfide-sulfate temperatures are shown in Fig. 4. The intermediate group samples give values varying from 500 °C to 600 °C and the felsic samples yield temperatures from 570 °C to 640 °C. Overall, the low equilibrium temperatures can be explained if the dark rims formed by subsolidus exsolution of nanoscale sulfide particles at temperatures of $\sim 500\text{--}650$ °C.

5.3. The high $\delta^{34}\text{S}$ of Etinde magmas

By disregarding the samples affected by degassing, the bulk-rock $\delta^{34}\text{S}$ range which best represents Etinde magmas is +3.7‰ to +6.3‰. These values are much higher than the well-constrained MORB range of -2.0% to -1.0% (Labidi et al., 2013) and higher than most other alkali igneous rocks (Hutchison et al., 2019). A recent global compilation of sulfur-isotope data in alkali igneous rocks shows these to range between -5.0 and $+2.0\%$ (Hutchison et al., 2019). The broad $\delta^{34}\text{S}$ range reported by Hutchison et al. (2019) reflects the wide variety of potential recycled components in the varied mantle source regions of alkali magmas.

It is possible that magma accumulating in reservoirs near the interface between low-density sedimentary rocks and the underlying higher-density continental or oceanic crust could have interacted with anhydrite (CaSO₄), either by bulk assimilation or by isotopic exchange. The $\delta^{34}\text{S}$ of evaporite deposits formed by evaporation of ~ 105 Ma seawater would have a value of around +16‰ (Paytan et al., 2004). Assimilation of only $\sim 0.5\%$ anhydrite in a magma with typical normal upper mantle (MORB-like) $\delta^{34}\text{S}$ could drive the magmatic $\delta^{34}\text{S}$ up to the range observed at Etinde (Fig. 7). Such a small addition would have no significant effect on the bulk magma composition. This explanation of evaporite assimilation has been invoked for the h a yne-bearing rocks of Vulsini, which erupted through carbonate and anhydrite deposits and also have positive $\delta^{34}\text{S}$ (+10 to +13‰, Renzulli et al., 1998). However, Aptian salt deposits on the African margin are restricted to locations well



Fig. 6. Left, Haiüyne-phyric intermediate nephelinite C228. Right, Nosean-phyric felsic nephelinite C231. Both shown in plane-polarised light. The pale blue haiüyne phenocrysts (left) have dark rims whereas the colourless nosean phenocrysts have dark cores (right). (For interpretation of the references to colour in this figure legend, the reader is referred to the web version of this article.)

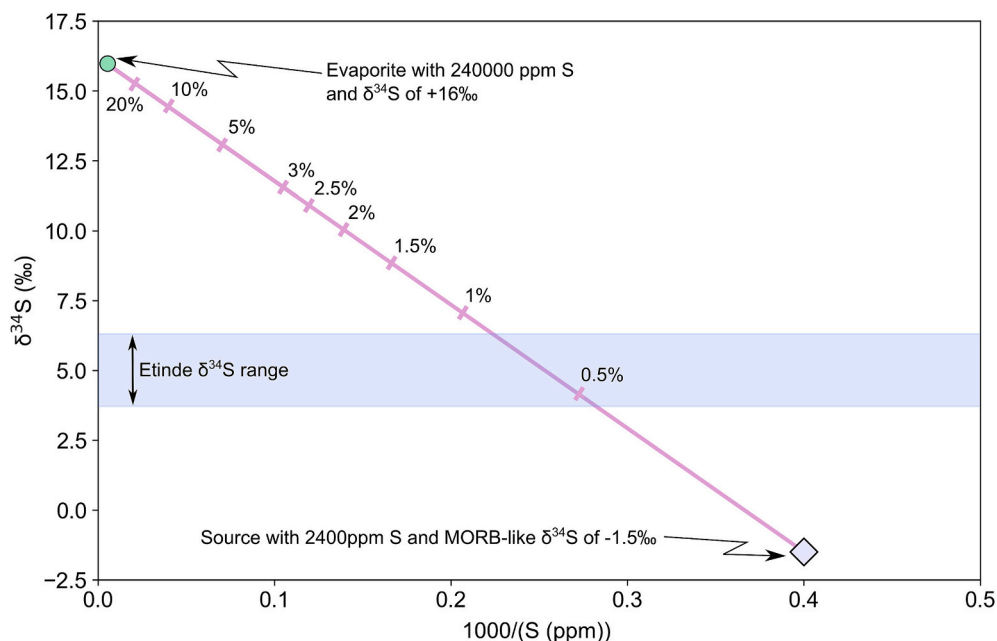


Fig. 7. The effect of assimilation of anhydrite with 23.5 wt% sulfur and $\delta^{34}\text{S}$ (+16 ‰). The Etinde data are represented by the pale blue area; the range of sulfur content in the magma is uncertain because of accumulation of haiüyne and nosean phenocrysts. (For interpretation of the references to colour in this figure legend, the reader is referred to the web version of this article.)

south of the CVL (Chaboureaux et al., 2012). Thus, although evaporite assimilation cannot be completely ruled out, it appears unlikely to be the cause of high $\delta^{34}\text{S}$ in the Etinde magmas.

We suggest that the high $\delta^{34}\text{S}$ in the Etinde magmas is an intrinsic feature of the enriched mantle source. The Etinde nephelinites not only have some of the highest recorded $\delta^{34}\text{S}$ but are also among the most highly silica-undersaturated and incompatible element-enriched igneous rocks worldwide. High $\delta^{34}\text{S}$ is a feature of low-temperature fractionation of sulfur and so implies recycling-driven mantle enrichment processes. A similar conclusion was reached by Marini et al. (1994) for the Vulture (Italy) haiüyne-bearing potassic volcanic rocks whose primitive magma had $\delta^{34}\text{S}$ estimated to be +4.0 ‰, close to the lower end of the range in the Etinde samples.

The Guimarães et al. (2020) model for enigmatic intraplate magmatism requires the enrichment of the base of the lithospheric mantle in small-volume carbonate melt fractions over extended periods. This

enriched zone becomes thickened during supercontinent formation and is subsequently converted to asthenosphere through thermal re-equilibration but is held in place through buoyancy until supercontinent break-up allows it to flow outwards. Melting of this enriched asthenosphere by decompression into lithosphere thin spots is a viable mechanism for persistent intraplate magmatism.

The role of carbonate-enriched mantle in the generation of alkaline magmas has been applied to many other intraplate magmatic provinces such as the East African rift (e.g. Hudgins et al., 2015) and the central European hotspots (e.g. Brandl et al., 2015), but always through in-situ melting of lithospheric mantle. The Guimarães et al. (2020) model is different in that the enriched mantle is mobilised and can flow out from beneath the continents into oceanic regions, as in the CVL. The model does not specify the source of the carbon in the enriching melt, specifically whether it is an intrinsic component of the mantle or is introduced into the mantle via recycling. The high $\delta^{34}\text{S}$ in the Etinde magmas shows

that at least some component of the enriched source is related to recycling-driven (subduction) processes that was added to the subcontinental mantle during the assembly of Pangea.

The model has far-reaching implications for the causes of intraplate magmatism. Break-up of Pangea and opening of the South Atlantic in the Cretaceous accompanied by outflow of enriched asthenospheric mantle can account for the CVL and the compositional similarity of its oceanic and continental sectors (Fitton and Dunlop, 1985) as well as the contemporaneous magmatism on the conjugate margin in Brazil (Guimarães et al., 2020). It is significant that the majority of ‘cold’ and ‘warm’ hotspots identified by Bao et al. (2022) are confined to the Atlantic and Indian Oceans, both of which opened during the break-up of Pangea, suggesting that the Guimarães et al. (2020) model may be widely applicable to enigmatic intraplate magmatism.

6. Conclusions

1. Etinde nephelinite magmas are highly enriched in incompatible elements and volatiles.
2. Degassing-induced fractionation of sulfur isotopes reduced the $\delta^{34}\text{S}$ of the most primitive magmas so they no longer represent the mantle source region.
3. The intermediate and felsic samples most faithfully record the magmatic $\delta^{34}\text{S}$ because they contain S-rich feldspathoid phenocrysts (haiyüne and nosean).
4. Sub-solidus exsolution of nanoscale sulfide particles in the S-rich feldspathoid phenocryst rims and cores can account for the low temperatures implied by the fractionation of sulfur isotopes between sulfate and sulfide phases.
5. The Etinde magmas had a $\delta^{34}\text{S}$ of range +3.7 ‰ to +6.3 ‰, which is higher than the MORB range and also higher than the typical $\delta^{34}\text{S}$ range of alkali magmas.
6. Assimilation of a small amount of anhydrite during storage in magma reservoirs could increase $\delta^{34}\text{S}$ and sulfur content, but this is unlikely to have caused the elevated $\delta^{34}\text{S}$ at Etinde because evaporite deposits on the West African margin have only been recorded well south of the CVL.
7. We suggest that the elevated $\delta^{34}\text{S}$ in the Etinde nephelinites is an intrinsic feature of their carbonate- and incompatible element-enriched mantle source and requires low-temperature fractionation of sulfur isotopes and the addition of this fractionated sulfur through subduction processes.
8. Our conclusions are widely applicable to other enigmatic intraplate magmatism where mantle plumes fail to provide a viable explanation.

CRedit authorship contribution statement

Sophie L. Baldwin: Writing – review & editing, Writing – original draft, Project administration, Methodology, Investigation, Funding acquisition, Formal analysis, Data curation, Conceptualization. **Linda A. Kirstein:** Writing – review & editing, Supervision, Methodology, Conceptualization. **J. Godfrey Fitton:** Writing – review & editing, Supervision, Methodology, Conceptualization. **Adrian J. Boyce:** Writing – review & editing, Methodology, Formal analysis. **William Hutchison:** Writing – review & editing, Supervision, Resources, Methodology, Formal analysis. **Michael A.W. Marks:** Writing – review & editing, Formal analysis. **Eva E. Stüeken:** Writing – review & editing, Formal analysis. **Chris Hayward:** Formal analysis.

Declaration of competing interest

The authors declare that they have no known competing financial interests or personal relationships that could have appeared to influence the work reported in this paper.

Acknowledgements

The authors thank Gavin Sim for facilitating sulfate sample preparation and Ivan Febrari for preparing polished thin sections. Insightful reviews by Zoltan Taracsak and one anonymous reviewer, as well as an informal review by Holly Elliot, greatly helped to improve the quality of this manuscript. We thank Claudia Romano for editorial handling. S. Baldwin acknowledges with thanks Lee Saper who helped guide thinking about $f\text{O}_2$ and the sulfur speciation-redox interplay. We also thank Fin Stuart for guidance with methodology and facilitating connections. S. Baldwin acknowledges funding from the E4 NERC doctoral training partnership (DTP) grant NE/S007407/1. W. Hutchison is funded by a UKRI Future Leaders Fellowship MR/S033505/1. E. Stüeken is funded by a NERC Frontiers grant NE/V010824/1. S. Baldwin publishes with the permission of the Executive Director of the British Geological Survey. For the purpose of open access, the author has applied a Creative Commons Attribution (CC BY) license to any Author Accepted Manuscript version arising from this submission.

Appendix A. Supplementary data

The supplementary material includes an Excel file with the XRF analyses of the Etinde sample suite as well as extended details about the methods used and the EMP sulfur K-alpha peak scans for the cores and rims of haiyüne and nosean phenocrysts. Supplementary data to this article can be found online at [<https://doi.org/10.1016/j.chemgeo.2025.122748>].

Data availability

All data in this study are publicly available through Mendeley Data at: <https://data.mendeley.com/datasets/pjtyzgxwwp/6>. The computational workbook for modelling fractionation due to degassing is available in the form of a Jupyter notebook at: <https://doi.org/10.5281/zenodo.10226648>.

References

- Bao, X., Lithgow-Bertelloni, C.R., Jackson, M.G., Romanowicz, B., 2022. On the relative temperatures of Earth's volcanic hotspots and mid-ocean ridges. *Science* 375 (6576), 57–61.
- Barfod, D.N., Ballentine, C.J., Halliday, A.N., Fitton, J.G., 1999. Noble gases in the Cameroon line and the He, Ne, and Ar isotopic compositions of high μ (HIMU) mantle. *J. Geophys. Res. Solid Earth* 104, 29509–29527.
- Baudouin, C., Parat, F., 2015. Role of volatiles (S, Cl, H₂O) and silica activity on the crystallization of haiyüne and nosean in phonolitic magmas (Eifel, Germany and Saghro, Morocco). *Am. Mineral.* 100, 2308–2322.
- Beaudry, P., Longpré, M.A., Economos, R., Wing, B.A., Bui, T.H., Stix, J., 2018. Degassing-induced fractionation of multiple sulphur isotopes unveils post-Archaeon recycled oceanic crust signal in hotspot lava. *Nat. Commun.* 9, 1–12.
- Berry, A.J., O'Neill, H.St.C., 2022. Oxygen content, oxygen fugacity, the oxidation state of iron, and mid-ocean ridge basalts. In: Moretti, R., Neuville, R.D. (Eds.), *Magma Redox Geochemistry*, Geophysical Monograph Series. American Geophysical Union, pp. 155–164.
- Brandl, P.A., Felix, S., Genske, F.S., Christoph Beier, C., Haase, K.M., Sprung, P., Krumm, S.H., 2015. Magmatic evidence for carbonate metasomatism in the lithospheric mantle underneath the Ohre (Eger) Rift. *J. Petrol.* 56, 1743–1774.
- Cabral, R.A., Jackson, M.G., Rose-Koga, E.F., Koga, K.T., Whitehouse, M.J., Antonelli, M. A., Farquhar, J., Day, J.M.D., Hauri, E.H., 2013. deep mantle storage of Archaeon crust. *Nature* 496, 490–493.
- Canfield, D.E., Raiswell, R., Westrich, J.T., Reaves, C.M., Berner, R.A., 1986. The use of chromium reduction in the analysis of reduced inorganic sulfur in sediments and shales. *Chem. Geol.* 54, 149–155.
- Chaboureaud, A.C., Donnadiou, Y., Sepulchre, P., Robin, C., Guillocheau, F., Rohais, S., 2012. The Aptian evaporites of the South Atlantic: a climatic paradox? *Climate of the Past* 8 (3), 1047–1058.
- Class, C., Goldstein, S.L., 2005. Evolution of helium isotopes in the Earth's mantle. *Nature* 436 (7054), 1107–1112.
- Coleman, M., Moore, M., 1978. Direct reduction of sulfates to sulfate dioxide for isotopic analysis. *Anal. Chem.* 50 (11), 1594–1595.
- De Moor, J.M., Fischer, T.P., Sharp, Z.D., King, P.L., Wilke, M., Botcharnikov, R.E., Cottrell, E., Zelenski, M., Marty, B., Klimm, K., Rivard, C., Ayalew, D., Ramirez, C., Kelley, K.A., 2013. Sulfur degassing at Erta Ale (Ethiopia) and Masaya (Nicaragua)

- volcanoes: Implications for degassing processes and oxygen fugacities of basaltic systems. *Geochemistry. Geophys. Geosystems* 14, 4076–4108.
- Dottin, J.W., Labidi, J., Lekic, V., Jackson, M.G., Farquhar, J., 2020. Sulfur isotope characterization of primordial and recycled sources feeding the Samoan mantle plume. *Earth Planet. Sci. Lett.* 534, 116073.
- Eggenkamp, H.G., Marks, M.A., Atanasova, P., Wenzel, T., Markl, G., 2020. Changes in halogen (F, Cl, Br, and I) and S ratios in rock-forming minerals as monitors for magmatic differentiation, volatile-loss, and hydrothermal overprint: The case for peralkaline systems. *Minerals* 10 (11), 995.
- Eldridge, D.L., Guo, W., Farquhar, J., 2016. Theoretical estimates of equilibrium sulfur isotope effects in aqueous sulfur systems: Highlighting the role of isomers in the sulfite and sulfoxylate systems. *Geochim. Cosmochim. Acta* 195, 171–200.
- Fitton, J.G., 1987. The Cameroon line, West Africa: a comparison between oceanic and continental alkaline volcanism. *Geol. Soc. Spec. Publ.* 30, 273–291.
- Fitton, J.G., Dunlop, H.M., 1985. The Cameroon line, West Africa, and its bearing on the origin of oceanic and continental alkali basalt. *Earth Planet. Sci. Lett.* 72, 23–38.
- Fitton, J.G., Saunders, A.D., Larsen, L.M., Hardarson, B.S., Norry, M.J., 1998. Volcanic rocks from the southeast Greenland margin at 63°N: composition, petrogenesis and mantle sources. *Proceed. Ocean Drilling Progr. Sci. Results* 152, 331–350.
- Geldmacher, J., Hoernle, K., Bogaard, P.V.D., Duggen, S., Werner, R., 2005. New ⁴⁰Ar/³⁹Ar age and geochemical data from seamounts in the Canary and Madeira volcanic provinces: Support for the mantle plume hypothesis. *Earth Planet. Sci. Lett.* 237, 85–101.
- Guimarães, A.R., Fitton, J.G., Kirstein, L.A., Barfod, D.N., 2020. Contemporaneous intraplate magmatism on conjugate South Atlantic margins: A hotspot conundrum. *Earth Planet. Sci. Lett.* 536, 116147.
- Halliday, A.N., Davidson, J.P., Holden, P., DeWolf, C., Lee, D.C., Fitton, J.G., 1990. Trace-element fractionation in plumes and the origin of HIMU mantle beneath the Cameroon line. *Nature* 347, 523–528.
- Head, E.M., Shaw, A.M., Wallace, P.J., Sims, K.W.W., Carn, S.A., 2012. Insight into volatile behavior at Nyamuragira volcano (D.R. Congo, Africa) through olivine-hosted melt inclusions. *Geochemistry. Geophys. Geosystems* 12, 1–22.
- Herzberg, C., Asimow, P.D., Arndt, N., Niu, Y., Leshner, C.M., Fitton, J.G., Cheadle, M.J., Saunders, A.D., 2007. Temperatures in ambient mantle and plumes: Constraints from basalts, picrites, and komatiites. *Geochem. Geophys. Geosyst.* 8.
- Hettmann, K., Wenzel, T., Marks, M., Markl, G., 2012. The sulfur speciation in S-bearing minerals: New constraints by a combination of electron microprobe analysis and DFT calculations with special reference to sodalite-group minerals. *Am. Mineral.* 97, 1653–1661.
- Hudgins, T.R., Mukasa, S.B., Simon, A.C., Moore, G., Barifajio, E., 2015. Melt inclusion evidence for CO₂-rich melts beneath the western branch of the East African Rift: implications for long-term storage of volatiles in the deep lithospheric mantle. *Contrib. Mineral. Petrol.* 169, 46.
- Hutchison, W., Babiak, R.J., Finch, A.A., Marks, M.A.W., Markl, G., Boyce, A.J., Stüeken, E.E., Friis, H., Borst, A.M., Horsburgh, N.J., 2019. Sulphur isotopes of alkaline magmas unlock long-term records of crustal recycling on Earth. *Nat. Commun.* 10, 4208.
- Hutchison, W., Finch, A.A., Borst, A.M., Marks, M.A.W., Upton, B.G.J., Zerkle, A.L., Stüeken, E.E., Boyce, A.J., 2021. Mantle sources and magma evolution in Europe's largest rare earth element belt (Gardar Province, SW Greenland): New insights from sulfur isotopes. *Earth Planet. Sci. Lett.* 568, 117034.
- Jenner, F.E., O'Neill, H.C. St, 2012. Analysis of 60 elements in 616 ocean floor basaltic glasses. *Geochem. Geophys. Geosyst.* 13, Q02005.
- Kirstein, L.A., Walowski, K.J., Jones, R.E., Burgess, R., Fitton, J.G., De Hoog, J.C.M., Savov, I.P., Kalnins, L.M., 2023. Volatiles and Intraplate Magmatism: a Variable Role for Carbonated and Altered Oceanic Lithosphere in Ocean Island Basalt Formation. *J. Petrol.* 64, 1–21.
- Labidi, J., Cartigny, P., Birc, J.L., Assayag, N., Bourrand, J.J., 2012. Determination of multiple sulfur isotopes in glasses: A reappraisal of the MORB 834S. *Chem. Geol.* 334, 189–198.
- Labidi, J., Cartigny, P., Moreira, M., 2013. Non-chondritic sulphur isotope composition of the terrestrial mantle. *Nature* 501, 208–211.
- Labidi, J., Cartigny, P., Jackson, M.G., 2015. Multiple sulfur isotope composition of oxidized Samoan melts and the implications of a sulfur isotope “mantle array” in chemical geodynamics. *Earth Planet. Sci. Lett.* 417, 28–39.
- Macdonald, G.A., Katsura, T., 1964. Chemical composition of Hawaiian lavas. *J. Petrol.* 5, 82–133.
- Marini, L., Paiotti, A., Principe, C., Ferrara, G., Cioni, R., 1994. Isotopic ratio and concentration of sulfur in the undersaturated alkaline magmas of Vulture Volcano (Italy). *Bull. Volcanol.* 56, 487–492.
- Marini, L., Chiappini, V., Cioni, R., Cortecchi, G., Dinelli, E., Principe, C., Ferrara, G., 1998. Effect of degassing on sulfur contents and 834S values in Somma-Vesuvius magmas. *Bull. Volcanol.* 60, 187–194.
- Marini, L., Moretti, R., Accornero, M., 2011. Sulfur isotopes in magmatic-hydrothermal systems, melts, and magmas. *Rev. Mineral. Geochem.* 73, 423–492.
- McKenzie, D., 1989. Some remarks on the movement of small melt fractions in the mantle. *Earth Planet. Sci. Lett.* 95, 53–72.
- Moussallam, Y., Oppenheimer, C., Scaillet, B., 2019. On the relationship between oxidation state and temperature of volcanic gas emissions. *Earth Planet. Sci. Lett.* 520, 260–267.
- Njome, M.S., De Wit, M.J., 2014. Earth-Science Reviews The Cameroon Line: Analysis of an intraplate magmatic province transecting both oceanic and continental lithospheres: Constraints, controversies and models. *Earth Sci. Rev.* 139, 168–194.
- Nkumbou, C., Déruelle, B., Velde, D., 1995. Petrology of mt etinde nephelinite series. *J. Petrol.* 36, 373–395.
- Ntombé, M., Déruelle, B., Mbowou, I.B.G., Ngounou, I., 2016. New Petrological and Geochemical Data of the Nephelinitic Lavas and Geodynamic Implications of Mount Etinde (Cameroon). *Int. J. Geosci.* 07, 1452–1470.
- O'Neill, H.St.C., Mavrogenes, J.A., 2022. The sulfate capacities of silicate melts. *Geochim. Cosmochim. Acta* 334, 368–382.
- Paytan, A., Kastner, M., Campbell, D., Thieme, M.N., 2004. Seawater sulfur isotope fluctuations in the Cretaceous. *Science* 304, 1663–1665.
- Putirka, K.D., 2005. Mantle potential temperatures at Hawaii, Iceland, and the mid-ocean ridge system, as inferred from olivine phenocrysts: Evidence for thermally driven mantle plumes. *Geochemistry. Geophys. Geosystems* 6 (5).
- Renzulli, A., Upton, B.G.J., Boyce, A., Ellam, R.M., 1998. Petrology of quartz syenite and haune syenite clasts from the Pitigliano Formation, Latera caldera, Vulturno District, Central Italy. *Eur. J. Mineral.* 10, 333–354.
- Rohde, J.K., van den Bogaard, P., Hoernle, K., Hauff, F., Werner, R., 2013. Evidence for an age progression along the Tristan-Gough volcanic track from new ⁴⁰Ar/³⁹Ar ages on phenocryst phases. *Tectonophysics* 604, 60–71.
- Saal, A.E., Hauri, E.H., 2021. Large sulfur isotope fractionation in lunar volcanic glasses reveals the magmatic differentiation and degassing of the Moon. *Sci. Adv.* 7, 1–11.
- Stuart, F.M., Lass-Evans, S., Godfrey Fitton, J., Ellam, R.M., 2003. High ³He/⁴He ratios in picritic basalts from Baffin Island and the role of a mixed reservoir in mantle plumes. *Nature* 424 (6944), 57–59.
- Suh, C.E., Luhr, J.F., Njome, M.S., 2008. Olivine-hosted glass inclusions from Scoriae erupted in 1954–2000 at Mount Cameroon volcano, West Africa. *J. Volcanol. Geotherm. Res.* 169, 1–33.
- Sun, S.S., McDonough, W.F., 1989. Chemical and isotopic systematics of oceanic basalts: Implications for mantle composition and processes. *Geol. Soc. Spec. Publ.* 42, 313–345.
- Taracsák, Z., Hartley, M.E., Burgess, R., Edmonds, M., Iddon, F., Longpré, M.-A., 2019. High fluxes of deep volatiles from ocean island volcanoes: Insights from El Hierro, Canary Islands. *Geochim. Cosmochim. Acta* 258, 19–36.
- Tian, D., Uieda, L., Leong, W.J., Schlitzer, W., Fröhlich, Y., Grund, M., Jones, M., Toney, L., Yao, J., Magen, Y., Tong, J.-H., Materna, K., Belem, A., Newton, T., Anant, A., Ziebarth, M., Quinn, J., Wessel, P., 2023. PyGMT: A Python interface for the Generic Mapping Tools.
- Wessel, P., Luis, J.F., Uieda, L., Scharroo, R., Wobbe, F., Smith, W.H.F., Tian, D., 2019. The Generic Mapping Tools Version 6. *Geochemistry. Geophys. Geosystems* 20, 5556–5564.
- White, W.M., Jackson, M.G., Hardardottir, S., 2025. Insights into mantle plume geochemistry from machine learning. *Geochem. Geophys. Geosyst.* 26, e2024GC011870.
- Willhite, L.N., Arevalo Jr., R., Piccoli, P., Lassiter, J.C., Rand, D., Jackson, M.G., et al., 2024. Oxygen fugacity of global ocean island basalts. *Geochem. Geophys. Geosyst.* 25, e2023GC011249.